Sub-GeV dark matter searches with EDELWEISS & CRYOSEL

Elsa Guy[a,*]**for the EDELWEISS, RICOCHET & CRYOSEL collaborations**

[a]*Univ Lyon, Université Lyon 1, CNRS/IN2P3, IP2I-Lyon, F-69622, Villeurbanne, France*

E-mail: e.guy@ip2i.in2p3.fr

The EDELWEISS collaboration searches for light Dark Matter (DM) particles using germanium detectors equipped with a charge and phonon signal readout. To circumvent the problem of the large background of events with no ionization signal ("Heat-Only" events) that limits the sensitivity of our detectors equipped with Ge-NTD sensors, the collaboration has tested the use of NbSi Transition Edge Sensors (TES). A moderate reduction has been observed and further improvements have been more recently obtained by exploiting the phonon yield from the Neganov-Luke-Trofimov (NTL) effect to better resolve electron recoils from HO events. These results pave the way for a new detector design, named CRYOSEL, that is being optimized for such a discrimination. The first results obtained with an early prototype are presented.
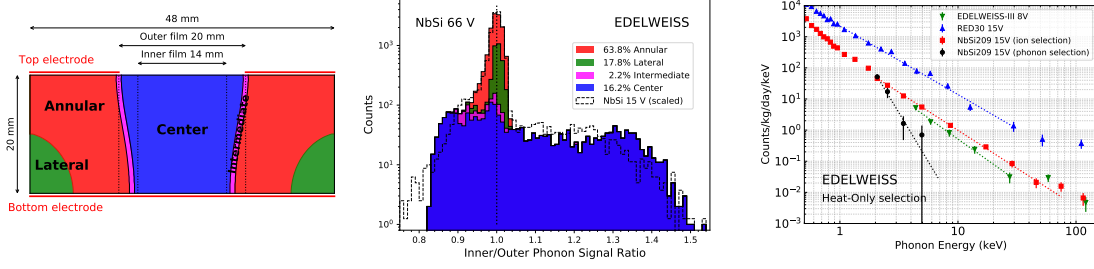
28.08-01.09.2023
University of Vienna

*Speaker

Introduction

There exist many theoretical models of dark matter (DM) particles. Within the very wide energy range from 1 eV/c² to 1 TeV/c², they can have detectable interactions with other particles [1–3]. Although big improvements in sensitivity have been achieved in detecting DM-nuclei or DM-electron interactions in the GeV/c² to TeV/c² scale, the absence of signal [4–8] has encouraged a lot of collaborations to turn to new technologies to detect lighter DM particles, in particular below 1 GeV/c² [9–15]. This lower energy range comes with new challenges such as unidentified low-energy backgrounds appearing in cryogenic experiments [16]. In the cryogenic detectors of the EDELWEISS collaboration, these backgrounds take the form of events not associated with the production of charges. Called *Heat-Only* (HO) events, they constitute the main element limiting the experiment sentivity [17–19].

1. Context

The EDELWEISS collaboration uses germanium (Ge) bolometers equipped with both charge and phonon readout to detect the interaction of a DM particle with either a nucleus of Ge or its electronic cloud. As part of a joint R&D program with the RICOCHET collaboration, the EDELWEISS collaboration is working on its Sub-GeV program with the objective of improving its resolution and sensivity to the eV-GeV/c² range. So far, a 17 eV resolution was achieved on the phonon channel by reducing the mass of detectors equipped with a Ge Neutron Transmutation Doped (Ge-NTD) phonon sensor [20]. A 1.6 eV resolution for the energy of electron recoils (ER) was achieved by applying a high voltage (HV) using the Neganov-Trofimov-Luke (NTL) amplification [21] on that same type of detector [18] equipped with a Ge-NTD. Indeed, the total phonon energy measured is $E_{phonon} = E_{recoil} + E_{NTL}$. The heat energy produced at the moment of the interaction is E_{recoil}, while E_{NTL} is another contribution to the phonon energy due to the NTL amplification. When a number N of $e^- h^+$ pairs drift through the crystal under the effect of an applied bias $|\Delta V|$, they interact with the crystal lattice producing additional phonons of energy $E_{NTL} = Ne\Delta V$ (where e is the elementary charge). The total gain accounting for the NTL effect is $\langle g \rangle = 1 + e\Delta V/\epsilon_\gamma$, where $\epsilon_\gamma = 3.0$ eV is the average ionization energy to produce a pair in Ge for ER [22].

To study the effect of the type of phonon readout on the measured background, a detector equipped with an NbSi Transition Edge Sensor (TES) sensitive to athermal phonons was then used to extract a new DM-nucleon interaction exclusion limit using Migdal effect [19]. Although the overall HO background measured with the NbSi TES was less than that measured with Ge-NTDs, it remains the dominant background. Hence, detecting athermal ballistic phonons (as opposed to the fully-thermalized phonons detected by the Ge-NTDs) is not sufficient to discriminate against the HO background. One hypothesis to remove this background would be to detect the presence of a single charge in the detector, taking advantage of the nature of HO events. An ionization resolution result in the 30 eV_{ee} range was achieved thanks to three 40 grams detectors read out using High Electron Mobility Transistors (HEMTs) [23]. Despite being seven to eleven times better than EDELWEISS-III performance [24] and allowing a large gain in events discrimination, it is not sufficient to extend the identification of charge to the domain of the single $e^- h^+$ pair needed to

Figure 1: *Left*: Scheme of the geometry of the NbSi films and the electrodes. The colors represent the different volumes bounded by the field lines. *Center*: Ratio r of the amplitude of the inner and outer film phonon signal for the different event categories of Fig. 1 (left). The categories are shown using the same color code. *Right*: Efficiency-corrected spectra of Heat-Only events selected by removing events with positive ionization signals. Green: EDELWEISS-III 0.82 kg detector; blue: the 33.4 g RED30 detector; and red: the NbSi209 0.20 kg detector. The efficiency-corrected spectra obtained with the NbSi209 detector by using the phonon cut ($r > 1.2$) instead is shown in black. The dotted lines are power-law fits to guide the eyes. [25]

handle the HO problem. Tagging the presence of charges using the electrode readout is thus, not yet an option for the needed energy scale. On the other hand, charges can be tagged indirectly by tagging the NTL phonons created as they drift under the effect of an electric field.
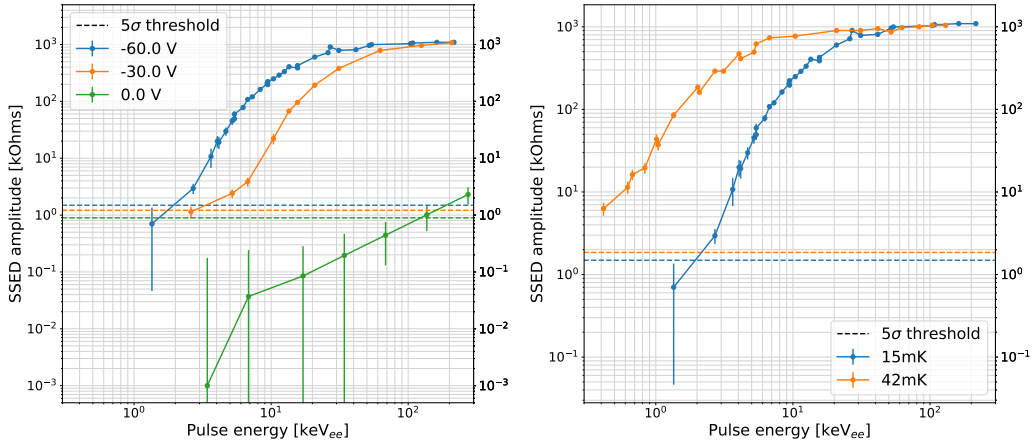
2. Tagging NTL phonons

The detector used to detect NTL phonons is called NbSi209. It is a 200 g Ge cylindrical bolometer equipped with top and bottom grid aluminum (Al) electrodes to measure the ionization signal. The top Al electrode does not cover the entire surface of the crystal, leaving a free area for the phonon sensor : in this case, the NbSi209 is equipped with an NbSi TES sensitive to athermal phonons. The NbSi film is lithographed in the shape of a spiral in the Al-free area of the top face of the crystal. The spiral is divided into two parts of equal resistance and read as two different sensors : the inner and outer films which dimensions are shown on Fig. 1 (left). More details on the experimental and acquisition setups are presented in [25]. The geometry of NbSi209 Al electrodes allows to discriminate between populations of events occurring in different volumes of the crystal : the lateral, annular, intermediate and central parts of the detector represented by different colors on Fig. 1 (left). For instance, charged events which ionization signal is fully collected by the bottom Al electrode, and not at all by the top annular electrode, are considered to be events from the central blue volume of Fig. 1, i.e., the volume under the NbSi TES. Looking at the ratio r of energy deposited on the inner and outer NbSi films ($r = E_{inner}/E_{outer}$) was found to be a good indicator of the presence of short-range high-energy phonons, that is, athermal NTL phonons, emitted in the proximity of the TES. Indeed, an excess of energy is only present in one film at a time, suggesting that the other film is only sensitive to the down-converted phonon contribution common to both films. In particular, it is explicitly visible for events selected as coming from the central volume using the electrode signal. The spectrum of events as a function of r on Fig. 1 (center) shows a clear excess of energy deposit on the inner NbSi film ($r > 1.2$) that can point to a sensitivity to the NTL phonons produced by these events. On Fig. 1 (right), we present the efficiency-corrected spectra

of HO events selected by imposing $E_{ion} < 0$ for different detectors. In green, an 800 g EDW-III detector, in blue the 30 g detector from [18], in red the 200 g NbSi209 detector. By selecting the events with $r > 1.2$ from the red spectrum, we obtain the black spectrum. The three detectors were operated during the same cool-down. The athermal phonon sensor measurements display a reduced rate of HO compared to that of the 33 g Ge-NTD equipped detector, but comparable rate compared to the 800 g one. Using the NbSi phonon sensor is not sufficient to discriminate against HO events, on the other hand, applying a cut on r allows to significantly reduce the HO rate. Tagging athermal phonons allows to partially reject HO events. This opens the possibility of developing a new detector type able to detect the presence of charges produced within the crystal by tagging NTL phonons : the *CRYOSEL detectors*.
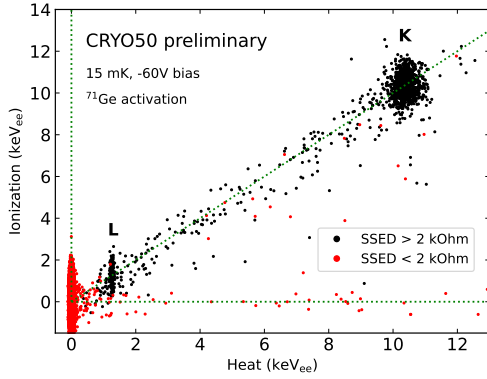
3. CRYOSEL

The CRYOSEL project relies on the development of bolometers equipped with a new sensor design called the Superconducting Single Electron Device (SSED) with the aim of tagging the presence of a single charge produced in the crystal. The CRYOSEL detectors are 40 g cylindrical Ge crystals with rounded edges, equipped with a Ge-NTD phonon sensor, Al electrodes for ionization readout and the SSED made of an NbSi line lithographed at the center of its top surface[26]. The electrodes and SSED are designed such as to constrain the field lines when applying an electric field to the detector, so that the created charge carriers drift towards the SSED. During their journey, the charges produce NTL phonons but the overwhelming majority of NTL athermal phonons is created in the very high field region in the vicinity of the SSED. The arrival of these high-energy phonons on a small section of the SSED ring loccaly triggers its superconducting-to-normal transition (T_c = 46 mK), giving an exploitable signal in the form of an increased resistance of the NbSi line R_{SSED} measured in kΩ, where the resistance of the entire film is 1 MΩ.

We present results obtained with the first operational SSED-equipped CRYOSEL detector called CRYO50, specifically, results on the SSED response to injected IR photon pulses. The details on the analysis and experimental setup are presented in [26]. The SSED response in kΩ to IR photon pulses of energy E_{Laser} was studied first by applying various biases $|\Delta V|$ with a fixed temperature of the detector T_{op} as shown on Fig 2 (left) and then by changing T_{op} and keeping $|\Delta V|$ constant as shown on Fig 2 (right). The absolute energy of the photon pulses was calibrated by comparing signal in the Ge-NTD and on the electrodes to those observed for ER events (see below and Fig 3). The dashed lines systematically correspond to the $5\sigma_{SSED}$ triggering threshold of the SSED, where σ_{SSED} is the SSED baseline resolution (RMS), of the corresponding color. The left panel of Fig 2 shows that the SSED signal exceeds the threshold only at high energy. This is not observed for point-like ER events in the bulk, indicating that the small non-zero signal in laser events is due to the presence in each burst of a few charges created very close to the electrodes. The blue and orange curves roughly display the same behaviors : below a certain value of E_{Laser}, it is not sufficient to trigger the SSED, this is called the *gap*. Then R_{SSED} rises with E_{Laser}, this is the *threshold mode*. Finally, both curves reach a plateau which corresponds to the *saturation mode*, where the entire NbSi ring has fully transitioned from superconducting to normal. An increased bias leads to a lower gap : indeed the SSED needs twice as less E_{Laser} to reach $R_{SSED} \approx 500 \, k\Omega$, that is, half its maximum resistance, when $|\Delta V|$ = 60 V (blue) compared to when $|\Delta V|$ = 30 V

Figure 2: SSED amplitude in kΩ as a function of the laser pulse energy in keV$_{ee}$. The SSED amplitudes are extracted from the mean value of the Gaussian fit of the amplitude distributions per laser energy. The vertical error bars correspond to the statistical uncertainty of the fit values. The dashed lines indicate the triggering threshold at $5\sigma_{SSED}$ where σ_{SSED} is the SSED baseline resolution (RMS). *Left*: Data taken at fixed $T_{op} = 15$ mK with $|\Delta V| = 0$ V in green, 30 V in orange and 60 V in blue. The SSED threshold at $5\sigma_{SSED}$ are 0.89 kΩ (green), 1.22 kΩ (orange), 1.49 kΩ (blue). *Right*: Data taken with fixed $|\Delta V| = 60$ V with $T_{op} = 15$ mK in blue and 42 mK in orange. The triggering threshold at $5\sigma_{SSED}$ are 1.49 kΩ (blue) and 1.85 kΩ (orange) for the two values of T_{op}. [26]

(orange). This scales with the number of NTL phonons produced, as it is multiplied by 2 when the bias is multiplied by 2. Hence, increasing the applied bias improves the SSED threshold. The blue curve on the right panel of Fig 2 is the same as the one on the left panel but this time compared to data taken with $T_{op} = 42$ mK with a fixed bias of $|\Delta V| = 60$ V. The temperature difference $\Delta T = T_c - T_{op}$ is a crucial parameter to veto the HO population. Operating CRYO50 at a higher temperature lowers the SSED trigger threshold because fewer phonons are needed to bridge the temperature gap ΔT.

Figure 3: CRYO50 ionization energy as a function of heat energy in keV$_{ee}$ for data taken at $T_{op} = 15$ mK and $|\Delta T| = 60$ V following ^{71}Ge activation. The K-shell and L-shell calibration peaks are visible at 10.37 keV$_{ee}$ and 1.3 keV$_{ee}$ respectively. The black dots correspond to events with $R_{SSED} > 2$ $k\Omega$, that is , events that have triggered the SSED. On the other hand, events with $R_{SSED} < 2$ $k\Omega$ (that did not trigger the SSED) are represented by red dots.

Lowering ΔT by either operating at a higher temperature and/or by reducing the critical temperature of the SSED line is another way of improving the SSED triggering threshold. Despite having a triggering threshold of several hundreds of $e^- h^+$ pairs [26], Fig. 3 shows that the CRYOSEL detectors can indeed discriminate against HO events by applying a cut on R_{SSED}. The data presented were taken at $T_{op} = 15$ mK with $|\Delta V| = 60$ V following ^{71}Ge activation. The black dots correspond to events for which $R_{SSED} > 2$ $k\Omega$, the K-shell and L-shell calibration peaks are visible at 10.37 keV$_{ee}$ and 1.3 keV$_{ee}$ respectively. The red dots are events for which $R_{SSED} < 2$ $k\Omega$, that is, events that did not pass the 5σ SSED triggering threshold. This cut on R_{SSED} allows to get rid of all events with $E_{ion} = 0$ keV$_{ee}$ which is a very promising first step for the CRYOSEL project.

Conclusion

We presented recent results achieved by both the EDELWEISS and RICOCHET collaborations to improve the sensitivity of cryogenic detectors. In regard to the HO background, the collaborations have described a technique able to tag charged events by detecting and localizing athermal phonons using NbSi TES. Inspired by these results, a new type of NbSi sensor was developed and tested with the objective of being able to tag the presence of a single charge to reject entirely the HO population of events down to energies where the resolution of the electrode readout is not sufficient. The first operational prototype equipped with this new SSED already showed promising results by allowing to remove events with no ionization. In the near future, CRYOSEL detectors will be part of a physics run within the BINGO experiment cryostat at LSM [27, 28]. On the long term, CRYOSEL detectors are proposed as an additional detector technology to TESSERACT experiment at LSM.

Acknowledgments

References

[1] M. W. Goodman, E. Witten, *Detectability of certain dark-matter candidates*, Phys. Rev. D. **31**, 3059 [`10.1103`].

[2] A. Drukier, K. Freese, D. N. Spergel, *Detecting cold dark-matter candidates*, Phys. Rev. D. **33**, 3495-3508 [`10.1103`].

[3] A. Drukier, L. Stodolsky, *Principles and applications of a neutral-current detector for neutrino physics and astronomy*, Phys. Rev. D. **30**, 2295 [`10.1103`].

[4] L. Bergström, *Non-baryonic dark matter: observational evidence and detection methods*, Rept. Prog. Phys. **63**, 793 [`hep-ph/0002126`].

[5] G. Bertone *et al.*, *Particle Dark Matter: Evidence, Candidates and Constraints*, Phys. Rep. **405**, 279 [`hep-ph/0404175`].

[6] E. Aprile *et al.* (XENON Collaboration), *Dark Matter Search Results from a One Ton-Year Exposure of XENON1T*, Phys. Rev. Lett. **121**, 111302 [`astro-ph/1805.12562`].

[7] D. S. Akerib *et al.* (LUX Collaboration), *Results from a Search for Dark Matter in the Complete LUX Exposure*, Phys. Rev. Lett. **118**, 021303 [`astro-ph/1608.07648`].

[8] X. Cui *et al.* (PandaX-II Collaboration) *Dark Matter Results from 54-Ton-Day Exposure of PandaX-II Experiment*, Phys. Rev. Lett. **119**, 181302 [`astro-ph/1708.06917`].

[9] M. Battaglieri *et al*, *US Cosmic Visions: New Ideas in Dark Matter 2017: Community Report*, arXiv:1707.04591 [`hep-ph/1707.04591`].

[10] G. Angloher *et al.* (CRESST Collaboration), *Results on light dark matter particles with a low-threshold CRESST-II detector*, Eur. Phys. J. C. **76**, 25 [`astro-ph/1509.01515`].

[11] D. W. Amaral *et al.*, *Constraints on low-mass, relic dark matter candidates from a surface-operated SuperCDMS single-charge sensitive detector*, Phys. Rev. D. **102**, 091101 [`hep-ex/2005.14067`].

[12] I. Alkhatib *et al.* (SuperCDMS Collaboration), *Light Dark Matter Search with a High-Resolution Athermal Phonon Detector Operated above Ground*, Phys. Rev. Lett. **127**, 061801 [`hep-ex/2007.14289`].

[13] A. Aguilar-Arevalo *et al.* (DAMIC Collaboration), *First Direct-Detection Constraints on eV-Scale Hidden-Photon Dark Matter with DAMIC at SNOLAB*, Phys. Rev. Lett. **118**, 141803 [`astrop-ph/1611.03066`].

[14] O. Abramoff *et al.* (SENSEI Collaboration), *SENSEI: Direct-Detection Constraints on Sub-GeV Dark Matter from a Shallow Underground Run Using a Prototype Skipper CCD*, Phys. Rev. Lett. **122**, 161801 [`hep-ex/1901.10478`].

[15] N.Castelló-Mor *et al.*, *DAMIC-M experiment: Thick, silicon CCDs to search for light dark matter*, Nucl. Instr. Meth. A. **958**, 162933 [`physics/2001.01476`].

[16] P. Adari *et al*, *EXCESS workshop: Descriptions of rising low-energy spectra*, arXiv:2202.05097 [`astrop-ph/2202.05097`].

[17] L. Hehn, *et al. Improved EDELWEISS-III sensitivity for low-mass WIMPs using a profile likelihood approach*, Eur. Phys. J. C. **76**, 548 [`astro-ph/1607.03367`].

[18] Q. Arnaud *et al.* (EDELWEISS Collaboration), *First Germanium-Based Constraints on Sub-MeV Dark Matter with the EDELWEISS Experiment*, Phys. Rev. Lett. **135**, 141301 [`astro-ph/2003.01046`].

[19] E. Armengaud *et al* (EDELWEISS Collaboration), *Search for sub-GeV dark matter via the Migdal effect with an EDELWEISS germanium detector with NbSi transition-edge sensors*, Phys. Rev. D. **106**, 062004 [`astro-ph/2203.03993`].

[20] E. Armengaud *et al* (EDELWEISS Collaboration), *Searching for low-mass dark matter particles with a massive Ge bolometer operated above ground*, Phys. Rev. D. **99**, 082003 [`astro-ph/1901.03588`].

[21] B. Neganov and V. Trofimov, *Colorimetric method measuring ionizing radiation*, Published in: Otkryt.Izobret. **146**, 215 (1985) [`USSR Patent No. 1037771`].

[22] G. F. Knoll, *Radiation Detection and Measurement*, 4th Edition, Wiley, Hoboken, 217, New York, 2010.

[23] C. Augier *et al* (EDELWEISS Collaboration), *First demonstration of 30 eVee ionization energy resolution with Ricochet germanium cryogenic bolometers*, arXiv:2306.00166 [`astro-ph/2306.00166`].

[24] E. Armengaud *et al.* (EDELWEISS Collaboration), *Performance of the EDELWEISS-III experiment for Dark Matter Searches*, JINST **12**, P08010 [`physics/1706.01070`].

[25] C. Augier *et al* (EDELWEISS Collaboration), *Tagging and localization of ionizing events using NbSi transition edge phonon sensors for dark matter searches*, Phys. Rev. D. **108**, 022006 [`physics/2303.02067`].

[26] H. Lattaud *et al Characterization of the phonon sensor of the CRYOSEL detector with IR photons*, arXiv:2311.01554 [`physics/2311.01554`].

[27] A. Armatol (BINGO Collaboration), *New results about the revolutionary bolometer assembly of BINGO*, arXiv:2301.06946 [`physics/2301.06946`].

[28] V. Berest (BINGO Collaboration), *BINGO: investigation of the Majorana nature of neutrinos at a few meV level of the neutrino mass scale*, in proceedings *TAUP 2023*.